Arch. Metall. Mater. **71** (2026), 2, 693-700

DOI: https://doi.org/10.24425/amm.2026.1438

D. VESELINOV[1*], V. KOEVA[1], R. YANKOVA[1], I. RUSEV[1], Y. YANKOV[1], H. SKULEV[1]

MICROSTRUCTURE, MICROHARDNESS AND WEAR BEHAVIOR OF TIN-BASED SURFACE LAYERS FORMED ON COMMERCIALLY PURE TITANIUM GRADES 2 AND 4 BY LASER PROCESSING

Laser surface modification under nitrogen was applied to commercially pure titanium (cpTi) Grade 2 and Grade 4 using a 455 nm diode laser at 30-90% of the nominal 22 W power. The evolution of microstructure, phase composition, hardness, and wear resistance was systematically evaluated. Cross-sectional analysis revealed the formation of a TiN-based compound layer whose thickness increased nonlinearly with laser power, from submicron scale at 30% to ~45 µm (Grade 2) and ~48 µm (Grade 4) at 90% power. X-ray diffraction confirmed TiN as the dominant phase, with increasing peak intensity corresponding directly to compound layer growth. Surface hardness increased markedly, reaching ~1675 HV in Grade 2 and ~1809 HV in Grade 4, compared to ~180-210 HV for the untreated substrates. Wear testing (0.5 kg load, 100 m sliding distance) demonstrated up to ~96% reduction in volume loss relative to low-power conditions. Optimal wear resistance was achieved at intermediate-to-high laser powers (50-70%), where a thick, continuous TiN-rich layer provided both high surface hardness and effective subsurface load support. These results demonstrate that laser processing under nitrogen enables controlled formation of functionally graded TiN-based layers on cpTi, with tribological performance governed primarily by compound layer thickness and hardness gradient continuity.

Keywords: Laser surface treatment; titanium nitriding; TiN; microhardness; wear resistance

1. Introduction

Commercially pure titanium (cpTi) and its alloys are widely used in biomedical applications owing to their excellent corrosion resistance, favorable biocompatibility, and suitable mechanical properties [1-3]. Among cpTi materials, Grades 2 and 4 are commonly employed for dental and orthopedic implants. Grade 2 is characterized by good ductility and corrosion resistance, whereas Grade 4 contains a higher oxygen content, leading to increased strength and hardness, which are particularly advantageous for load-bearing implant components [4]. Nevertheless, both grades suffer from relatively low surface hardness and limited wear resistance, which may result in surface damage and debris generation under tribological loading conditions [5,6].

To overcome these limitations, various surface modification techniques have been investigated to improve the surface performance of titanium without affecting its bulk properties. Thermochemical treatments such as nitriding and oxynitriding are of particular interest due to their ability to form hard ceramic surface layers, including titanium nitride (TiN) and oxygen-containing nitride phases, which significantly enhance hardness and wear resistance [6-8]. However, conventional nitriding and oxynitriding methods often require high processing temperatures, long treatment times, or complex controlled atmospheres, limiting their applicability to finished biomedical components [9,10].

Laser surface processing offers an attractive alternative for titanium surface modification. Owing to its high energy density and localized heat input, laser processing enables rapid surface melting and accelerated diffusion of reactive species while minimizing thermal effects on the substrate [11-13]. When titanium is laser processed under a nitrogen atmosphere, nitrogen readily reacts with the molten surface to form TiN. At the same time, oxygen originating from the native titanium oxide layer and residual oxygen or moisture in the processing environment may contribute to the formation of mixed nitride/oxynitride phases, often described as Ti(O,N) [14]. Such laser-induced nitride/oxynitride layers are typically characterized by a hard surface zone supported by a diffusion-affected region, resulting in improved tribological performance.

Despite extensive studies on laser nitriding of titanium, comparative investigations addressing the influence of cpTi grade on laser-induced phase formation and functional proper-

[1] INSTITUTE OF METAL SCIENCE, EQUIPMENT, AND TECHNOLOGIES WITH CENTER FOR HYDRO- AND AERODYNAMICS "ACAD. A. BALEVSKI", BULGARIAN ACADEMY OF SCIENCES, SOFIA, BULGARIA

* Corresponding author: dveselinov@ims.bas.bg

ties remain limited. In particular, the role of oxygen content in cpTi Grades 2 and 4 on microstructural evolution, hardness gradients, and wear behavior under laser processing conditions has not been fully clarified [15,16]. A systematic comparison of these materials is therefore necessary to optimize laser surface treatments for biomedical applications.

In this study, laser surface processing under a nitrogen jet was performed on cpTi Grades 2 and 4 using a diode laser system equipped with a custom gas delivery nozzle. The resulting surface layers were characterized in terms of cross-sectional microstructure, phase composition, microhardness distribution, and wear resistance. The aim of this work is to elucidate the formation of nitride/oxynitride layers under nitrogen atmosphere and to assess the influence of cpTi grade on the resulting microstructural and tribological performance.

2. Experimental

Commercially pure titanium alloys cpTi Grade 2 and cpTi Grade 4 were used as substrate materials in this study. The chemical composition of both alloys is provided in TABLE 1. Cylindrical specimens were machined with a diameter of 16 mm for Grade 2 and 12 mm for Grade 4, while the height of all samples was 5 mm. Prior to laser treatment, the samples were sequentially ground using SiC abrasive papers and subsequently polished with diamond suspensions to obtain a mirror-like surface finish. Surface cleaning and microstructural revelation were carried out by etching the polished samples in Kroll's reagent for 30 s. After etching, the specimens were thoroughly rinsed with distilled water and dried in ambient air before laser processing.

TABLE 1

Chemical composition of titanium alloys cpTi Grade 2 and cpTi Grade 4

Alloy	O (wt.%)	Fe (wt.%)	C (wt.%)	N (wt.%)	H (wt.%)	Ti
cpTi Grade 2	≤0.25	≤0.30	≤0.08	≤0.03	≤0.015	Balance
cpTi Grade 4	≤0.40	≤0.50	≤0.08	≤0.05	≤0.015	Balance

Laser surface treatment was performed using a diode laser system with a nominal output power of 22 W operating at a blue wavelength of 455 ± 5 nm. A custom-designed nozzle for reactive gas delivery was mounted coaxially to the laser head to supply nitrogen directly to the laser-material interaction zone. High-purity nitrogen gas (99.9999%) was used as the reactive atmosphere during laser processing, with the gas flow rate maintained constant at 25 L/min throughout all experiments. Laser irradiation was carried out at four different power levels corresponding to 30%, 50%, 70%, and 90% of the nominal laser output. The laser beam, with a spot diameter of approximately 100 μm, was scanned across the sample surface at a constant traverse speed of 1000 mm/min. To facilitate comparison with other studies, the linear energy input (line energy) was estimated based on the applied laser power and scanning speed. Considering the constant scanning speed of 1000 mm/min (16.67 mm/s), the corresponding line energy values were approximately 0.40 J/mm (30%), 0.66 J/mm (50%), 0.92 J/mm (70%), and 1.19 J/mm (90%). These values provide more direct representation of the energy input governing melt pool formation and nitrogen incorporation. All laser treatments were conducted under ambient laboratory conditions (temperature ~22 ± 2°C, relative humidity ~40-60%).

The microstructure and thickness of the laser-modified layers were examined by optical microscopy using an upright optical microscope equipped with a digital camera and dedicated image analysis software (LM-308, L&D; DGT-SRT200A, Dandong, China). Cross-sectional specimens were prepared using a low-speed precision cutting machine (DTQ-5, LaiZhou Weiyi Experimental Machinery Manufacture Co., Yantai, China). The sectioned samples, including both the modified layer and the substrate, were mounted in black resin, ground using alumina-based abrasive papers, and polished with diamond suspensions to achieve a scratch-free surface suitable for microstructural observation.

Phase composition of the laser-treated surfaces was analyzed by X-ray diffraction (XRD) using a Bruker D8 Discover diffractometer (Bruker, Billerica, MA, USA) with Cu Kα radiation (λ = 1.5406 Å) operated at room temperature. Diffraction patterns were recorded in coupled θ-2θ mode over a 2θ range of 20°-90°. Phase identification was performed using XRD analysis software (X'Pert HighScore Plus, PANalytical B.V., Almelo, The Netherlands) by comparison with standard reference patterns.

Microhardness profiles were measured using a DVK-200A microhardness tester equipped with a Vickers indenter. A load of 0.01 kg (100 g) was applied with a constant dwell time. Indentations were performed from the treated surface toward the substrate on polished cross-sections in order to evaluate the hardness gradient across the laser-modified layer and the underlying diffusion zone. Microhardness measurements were performed at least three times at each depth, and average values are reported. The variation between measurements was within ±5% for most data points.

The wear resistance of the laser-treated titanium surfaces was evaluated using a pin-on-flat configuration on a commercial tribometer (Glomro BXT-MAR306). A hardened steel ball (diameter 6.35 mm) was used as the counterbody. The tests were conducted under a normal load of 0.5 kg (≈4.9 N), with reciprocating sliding along a 20 mm stroke length for 5000 cycles, corresponding to a total sliding distance of 100 m. All tests were performed under ambient laboratory conditions. After testing, the wear tracks were examined by optical microscopy. The wear track width was measured at multiple locations along the sliding path and averaged. The wear volume was calculated from the measured track geometry using standard geometric relations for a spherical counterbody, assuming a circular cross-sectional profile of the wear scar.

3. Results and discussion

3.1. Microstructure

Fig. 1 presents cross-sectional optical micrographs of cpTi Grade 2 (A-D) and cpTi Grade 4 (E-H) after laser processing under a nitrogen atmosphere at power levels ranging from 30% to 90% of the nominal 22 W output. Independent of alloy grade, laser treatment produces a distinct multilayer architecture consisting of a bright, weakly etched surface compound layer, an intermediate fine acicular zone, and a deeper large acicular region, followed by the unaffected substrate. The thickness and morphology of these regions are strongly influenced by laser power and exhibit systematic differences between the two grades.

For cpTi Grade 2, the modified region at 30% power remains relatively shallow. A thin compound layer of approximately 0.8 μm is visible at the surface, indicating limited surface reaction under low energy input. Beneath this layer, a fine acicular zone (~3 μm) transitions into a larger acicular region extending to ~30 μm from the surface, resulting in a total modified depth of approximately 34 μm. The predominance of the acicular morphology and the limited thickness of the compound layer suggest a diffusion-assisted transformation regime with restricted melt pool development.

Increasing the laser power to 50% leads to a pronounced thickening of all modified zones. The compound layer increases to ~8 μm, while the fine and large acicular zones extend to ~10 μm and ~46 μm, respectively. The deeper thermal penetration and more developed acicular morphology indicate stable melt pool formation and enhanced nitrogen uptake. At 70% power, the compound layer grows markedly to ~30 μm, accompanied by a fine acicular zone of ~15 μm and a large acicular region reaching ~60 μm. The significant increase in compound thickness reflects intensified surface reactions during the molten state, although the emergence of surface undulations indicates increasing melt pool instability. At 90% power, the compound layer further thickens to ~45 μm and becomes morphologically irregular. The fine acicular zone (~17 μm) shows only a modest increase compared to 70%, whereas the large acicular region extends to ~70 μm. The total modified depth exceeds 130 μm, demonstrating substantial thermal influence.

A comparable multilayer structure is observed in cpTi Grade 4, though with consistently greater compound layer thickness at all power levels. At 30% power, the compound layer already reaches ~3 μm, approximately four times thicker than in Grade 2 under identical conditions, while the fine and large acicular zones measure ~4 μm and ~30 μm, respectively. Increasing the power to 50% produces a compound layer of ~16 μm, accompanied by fine and large acicular zones of ~12 μm and ~52 μm. At 70% power, the compound layer thickens to ~36 μm and the large acicular region extends to ~71 μm, while the fine acicular zone stabilizes near ~17 μm. Further increasing the power to 90% results in a compound layer thickness of

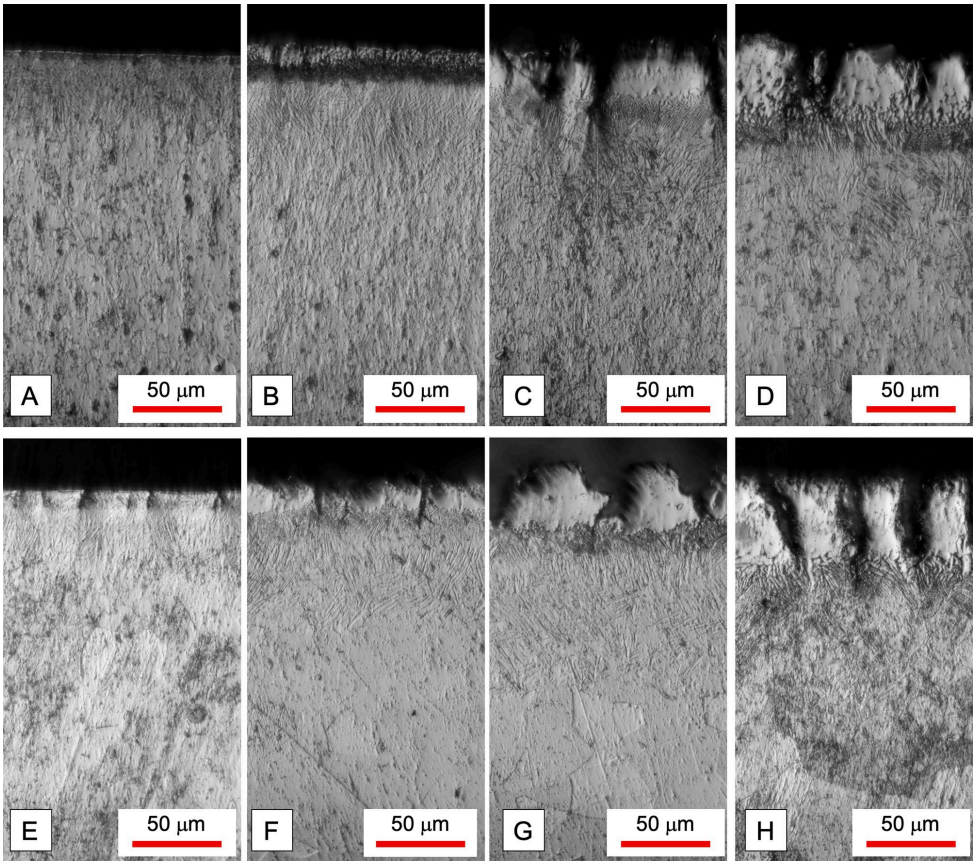

Fig. 1. Cross-sectional optical micrographs of laser-treated cpTi Grade 2 (A-D) and cpTi Grade 4 (E-H) processed under a nitrogen atmosphere at different laser power levels: 30% (A, E), 50% (B, F), 70% (C, G), and 90% (D, H) of the nominal 22 W output

~48 µm and a large acicular depth of ~76 µm, yielding a total modified region exceeding 140 µm. As in Grade 2, high power induces surface irregularities indicative of intensified melt pool convection and localized over-melting.

Direct comparison between the two grades reveals that the compound layer growth is systematically more pronounced in Grade 4 across all processing conditions, whereas the thickness of the acicular zones follows similar trends in both materials. The compound layer exhibits a strongly nonlinear increase with laser power, indicating that surface reaction kinetics are governed primarily by melt pool temperature and residence time. In contrast, the acicular transformation zones increase more gradually, reflecting their dependence on thermal gradients and rapid solidification dynamics. The consistently thicker compound layer observed in Grade 4 can be rationalized by its higher oxygen content (TABLE 1), which increases the concentration of interstitial solutes in the α-Ti matrix, modifies melt pool thermodynamics, and enhances the stabilization of nitrogen-containing phases during rapid solidification.

The microstructural evolution demonstrates a clear transition from a shallow, diffusion-influenced modification regime at 30% power to a melt-dominated reactive regime at 50% and above. At ≥70%, further power increase primarily enhances compound layer thickness and surface roughness without proportionally increasing the depth of the acicular zones, suggesting the existence of an optimal processing window for controlled nitride layer development.

3.2. XRD phase analysis

Fig. 2 presents the XRD patterns of cpTi Grade 2 and cpTi Grade 4 substrates and laser-treated samples processed under nitrogen at 30-90% of the nominal laser power. All measurements were performed in θ-2θ geometry using Cu Kα radiation.

The untreated substrates of both grades exhibit diffraction patterns characteristic of α-Ti (hcp), with dominant reflections corresponding to the (100), (002), (101), (102), (110), and higher-index planes. No secondary phases are detected, confirming that both materials are initially single-phase α-Ti prior to laser processing. Minor peak position variations are within experimental uncertainty.

Following laser irradiation under nitrogen, additional reflections emerge in all treated samples. The most diagnostic peaks appear at approximately 36.6°, 42-44°, 62-63°, and 74-76°, corresponding to the characteristic (111), (200), (220), and (311) reflections of face-centered cubic TiN. Slight shifts are observed particularly in the (200) region. The presence of TiN is detectable already at 30% power, although α-Ti peaks remain dominant, indicating that the modified layer is thin and that the diffraction signal is still strongly influenced by the substrate. This observation is consistent with the microstructural analysis, where the compound layer thickness at 30% power is below 1 µm.

With increasing power to 50% and 70%, the relative intensity of TiN reflections increases significantly, particularly in the (200) region near ~43-44° and in the (220) region near ~63°. This trend correlates directly with the measured increase in compound layer thickness from 8 µm (50%) to 30 µm (70%). At 90% power, TiN reflections become clearly pronounced relative to α-Ti, consistent with the formation of a ~45 µm thick compound layer.

A slight shift and broadening of TiN-related peaks, particularly the (111) and (200) reflections, are observed at higher powers. Such variations indicate lattice distortion and residual stresses associated with rapid melt-solidification. The deviation from ideal TiN peak positions may indicate the formation of non-stoichiometric TiN_x and possible Ti(O,N) solid solution due to oxygen incorporation. However, the presence of Ti(O,N) cannot be conclusively confirmed based on XRD alone and should be considered as a plausible interpretation. Additional techniques such as XPS or EDS would be required for definitive phase identification. A weak additional reflection near ~28-29°, absent in the substrate, indicates minor oxide formation (TiO_2-related), although its low intensity confirms that the surface remains predominantly nitride-dominated.

The phase evolution in cpTi Grade 4 follows a similar overall trend but with quantitatively enhanced nitride formation. TiN reflections are clearly visible already at 30% power

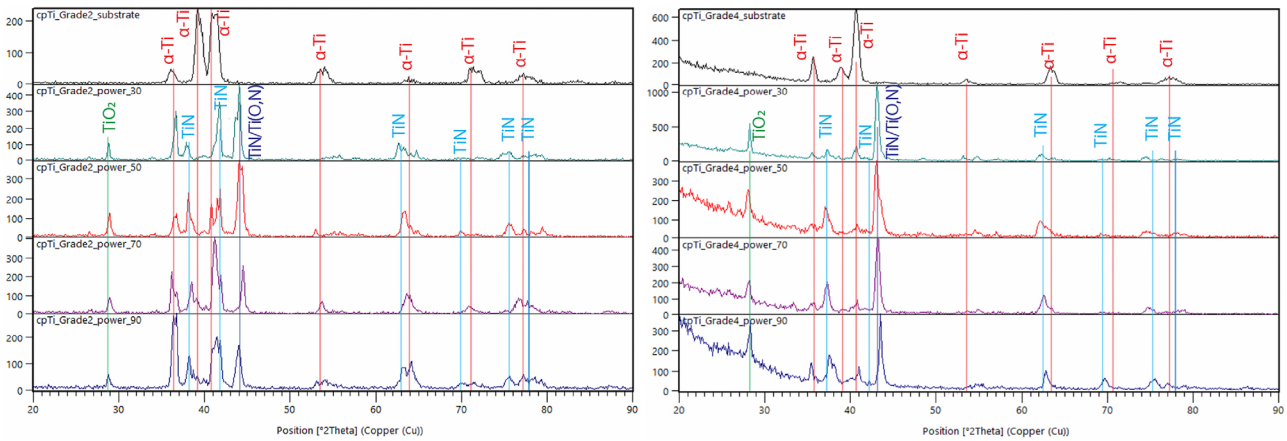

Fig. 2. XRD patterns of cpTi Grade 2 (left) and cpTi Grade 4 (right) substrates and samples laser-treated under nitrogen at 30%, 50%, 70%, and 90% of the nominal 22 W power

and exhibit higher relative intensity compared to Grade 2 at the same processing condition. This is consistent with the thicker compound layer observed in Grade 4 (~3 μm vs ~0.8 μm at 30% power).

At 50% and 70% power, TiN peaks become increasingly dominant. The growth in TiN peak intensity correlates closely with the measured compound layer thickness, which increases from 16 μm (50%) to 36 μm (70%). At 90% power, the TiN reflections are strongest, in agreement with the maximum compound layer thickness of ~48 μm.

Compared to Grade 2, the TiN-related peaks in Grade 4 exhibit slightly different positions and more pronounced asymmetry in the ~43-44° region. These differences indicate variations in lattice parameter and stress state, likely influenced by the higher oxygen content of Grade 4. The enhanced interstitial concentration likely promotes stabilization of nitrogen-containing phases and may facilitate Ti(O,N) formation during rapid solidification.

A direct correlation exists between the evolution of TiN diffraction intensity and the measured compound layer thickness in both alloys. The nonlinear increase in compound layer thickness with laser power is mirrored by the progressive intensification of TiN reflections. In contrast, α-Ti peaks decrease in relative prominence but remain detectable in all conditions, indicating that the X-ray penetration depth extends into the substrate even at the highest power levels.

The results demonstrate a clear transition from a diffusion-dominated regime at low power, where TiN formation is limited and substrate reflections dominate, to a compound-layer-dominated regime at ≥50% power. At higher powers (70-90%), further energy input primarily increases TiN layer thickness and residual stress without fundamentally altering the phase constitution.

The XRD analysis confirms that laser processing under a nitrogen jet leads to the formation of a TiN-based surface layer with minor oxide contributions. The thicker compound layers and stronger TiN reflections observed in Grade 4 are consistent with its higher interstitial oxygen content, which modifies melt pool thermodynamics and promotes enhanced stabilization of nitride and oxynitride phases during rapid solidification.

3.3. Microhardness

Fig. 3 presents the cross-sectional Vickers microhardness profiles (HV0.01) of laser-treated cpTi Grade 2 and cpTi Grade 4 as a function of depth from the processed surface. The first measurement point (5 μm) corresponds to the outermost region accessible to indentation. All treated conditions exhibit a pronounced near-surface hardness enhancement followed by a gradual decrease toward substrate values, confirming the formation of a graded hardened layer. The spacing between indentations was selected to minimize interaction between adjacent plastic deformation zones and to avoid overlap effects, particularly near the surface where steep hardness gradients are present.

For cpTi Grade 2, the hardness at 5 μm increases from 1149 HV at 30% power to 1654-1675 HV at 50-90% power. At 30% power, the compound layer thickness is below 1 μm. Therefore, the hardness values recorded at 5-10 μm predominantly reflect the nitrogen-enriched and rapidly transformed subsurface zone rather than the intrinsic response of a continuous compound layer. With increasing power (≥50%), the compound layer thickness increases significantly (8-45 μm), and the corresponding increase in TiN peak intensity in XRD is accompanied by a clear extension of the high-hardness region. While the maximum surface hardness tends to plateau above ~1600 HV, elevated hardness persists to progressively greater depths, remaining above ~1400 HV at 10 μm and above ~600-1450 HV at 30 μm depending on power.

A similar trend is observed for cpTi Grade 4, although the response is quantitatively different. Low-power treatments (30-50%) produce lower near-surface hardness (746-962 HV at 5 μm) and a relatively shallow hardened zone. In contrast, 70-90% power results in the highest surface hardness (1758-1809 HV at 5 μm) and a substantially deeper hardened region. This behavior correlates directly with the systematically thicker compound layers in Grade 4 (3-48 μm) and the stronger TiN reflections identified in the XRD analysis. In both materials, hardness values gradually approach the substrate level (~180-210 HV) beyond approximately 110-150 μm, indicating

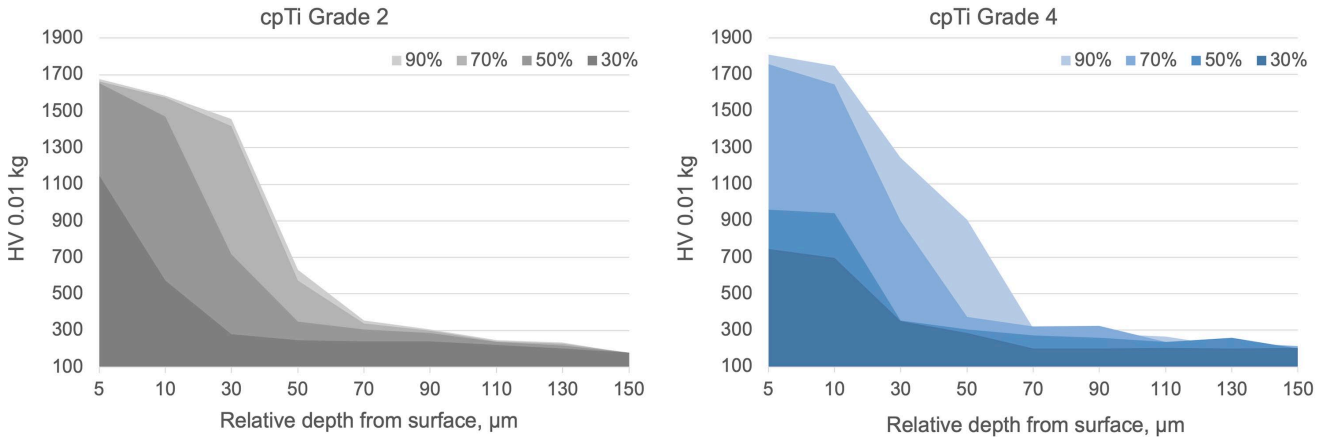

Fig. 3. Cross-sectional microhardness profiles (HV0.01) of cpTi Grade 2 (left) and cpTi Grade 4 (right) as a function of depth from the laser-treated surface under nitrogen at 30%, 50%, 70%, and 90% of the nominal 22 W power

that laser-induced strengthening remains confined to the near-surface region.

The hardness profiles correlate primarily with compound-layer thickness rather than solely with peak surface hardness. As the TiN-rich layer thickens with increasing laser power, the depth over which elevated hardness is maintained increases markedly. The near-surface hardness tends to saturate once a continuous TiN-based layer is established, whereas hardness at intermediate depths (30-50 μm) increases strongly with compound layer growth. This behavior is fully consistent with the microstructural observations and the power-dependent evolution of TiN identified by XRD.

3.4. Wear resistance

Fig. 4 shows representative optical micrographs of the wear tracks, while Fig. 5 summarizes the corresponding track width and calculated volume loss. The wear behavior strongly depends on laser power and alloy grade, reflecting the thickness and integrity of the TiN-based compound layer and the hardness gradients described in the previous sections.

For cpTi Grade 2, the 30% condition (Fig. 4A) exhibits a wide and relatively smooth wear scar with pronounced ploughing marks along the sliding direction, consistent with severe adhesive–abrasive wear of predominantly α-Ti. The large track width (0.68 mm) and high volume loss (0.08281 mm^3) confirm insufficient protection by the very thin compound layer (~0.8 μm).

At 50% and 70% power (Fig. 4B-C), the wear tracks become significantly narrower and more uniform. The ploughing grooves are reduced and the surface appears more compact, indicating that a continuous TiN-rich layer is effectively supporting the load. The corresponding volume losses decrease by nearly an order of magnitude (0.01032 and 0.00709 mm^3), correlating directly with the increased compound layer thickness (8-30 μm) and the strong TiN reflections observed in XRD.

At 90% power (Fig. 4D), the wear track is the narrowest (0.23 mm) and shows limited plastic smearing, confirming the highest wear resistance (0.00319 mm^3). The thick (~45 μm) TiN-based layer and extended high-hardness region provide both surface hardness and subsurface load support, minimizing material removal.

The wear behavior of cpTi Grade 4 follows a similar but more complex evolution. At 30% power (Fig. 4E), the wear track is wide (0.83 mm) and exhibits pronounced material removal with clear ploughing and smearing, resulting in the highest measured volume loss (0.15085 mm^3). Despite a slightly thicker compound layer than Grade 2 at this power, the lower near-surface hardness and limited load support lead to substantial plastic deformation.

At 50% and 70% power (Fig. 4F-G), the wear scars become markedly narrower and more uniform. The surface appears more compact, with reduced groove depth and limited mate-

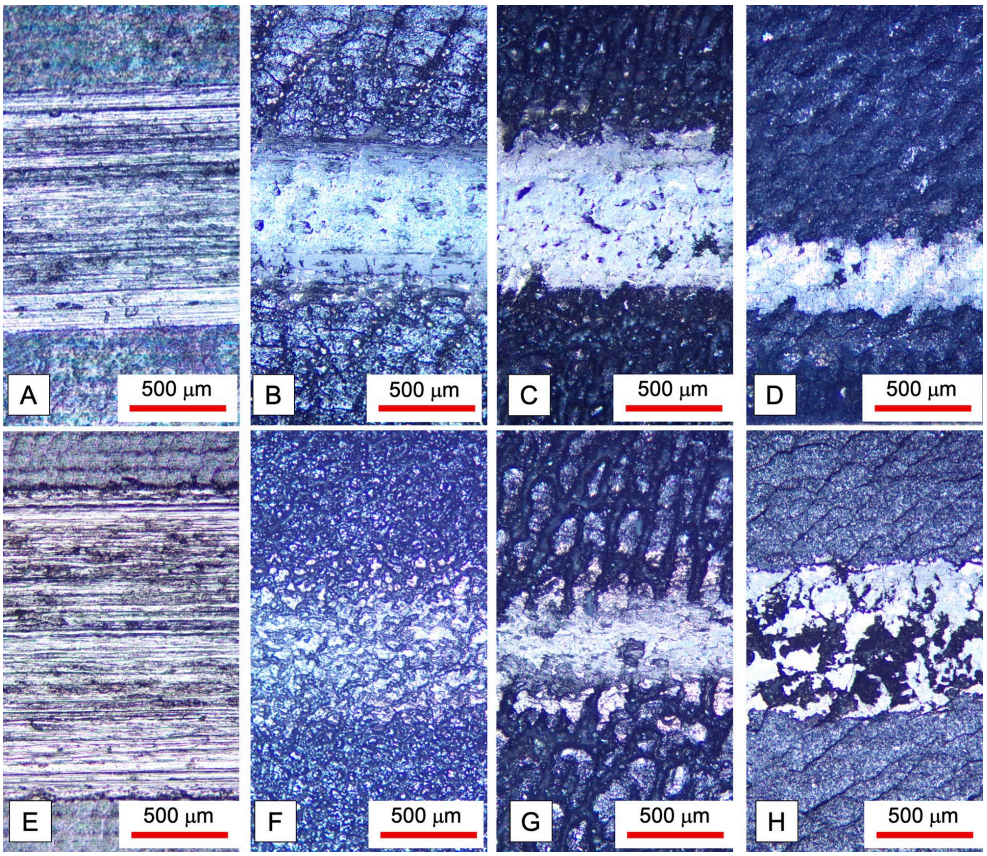

Fig. 4. Optical micrographs of wear tracks formed on laser treated cpTi Grade 2 (using power: A-30%, B-50%, C-70%, D-90%), and cpTi Grade 4 (using power: E-30%, F-50%, G-70%, H-90%) after 100 m sliding under a 0.5 kg load against a hardened steel ball (ϕ 6.35 mm)

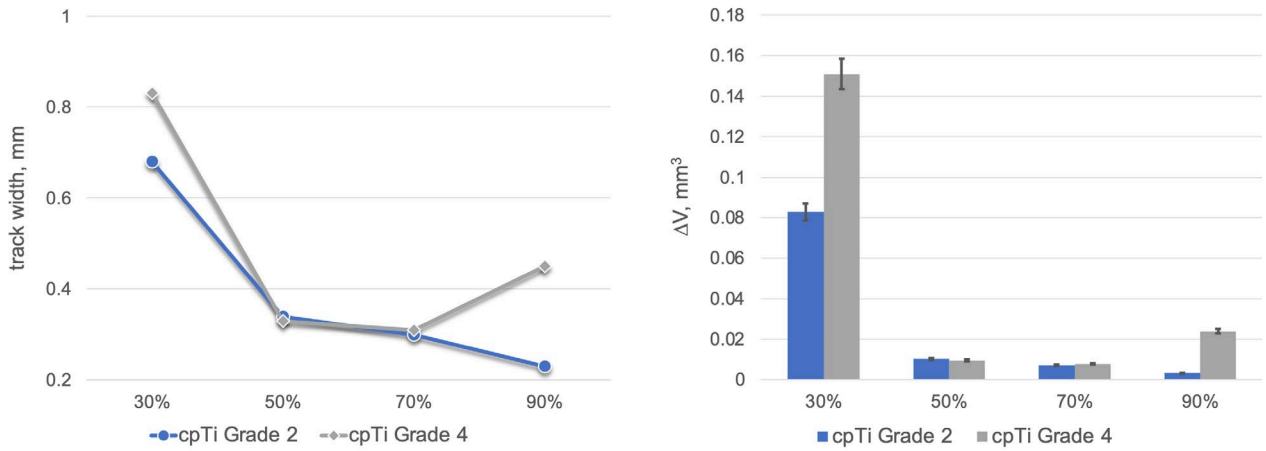

Fig. 5. Wear track width and calculated volume loss (ΔV) of laser-treated cpTi Grade 2 (using power: A-30%, B-50%, C-70%, D-90%), and cpTi Grade 4 (using power: E-30%, F-50%, G-70%, H-90%) after 100 m sliding under a 0.5 kg load against a hardened steel ball (ϕ 6.35 mm)

rial pull-out. Volume loss decreases dramatically to 0.00944 and 0.00782 mm^3, matching the performance of Grade 2 under similar conditions. These results coincide with the formation of thick (16-36 µm), continuous TiN-based layers and high surface hardness (≥1700 HV).

At 90% power (Fig. 4H), however, the wear scar becomes noticeably wider (0.45 mm) and shows localized fragmentation and discontinuities within the track. The corresponding increase in volume loss (0.02395 mm^3) suggests partial brittle fracture or micro-spallation of the compound layer. Although this condition exhibits the highest surface hardness (~1800 HV), excessive energy input likely increases residual stresses and surface roughness, reducing layer integrity during sliding. The observed degradation in wear performance at the highest power level is likely associated with increased residual stresses and local brittleness of the thick compound layer, as commonly reported for laser-treated titanium surfaces under high thermal input [11,15]. However, direct measurement of residual stresses was not performed in the present study and this interpretation should be considered indicative.

Taken together, the wear micrographs confirm that wear resistance correlates more strongly with compound layer continuity and load-bearing capacity than with peak hardness alone. When the TiN-rich layer is thin (30% power), wear is governed by substrate-controlled plastic deformation. At intermediate powers (50-70%), a thick and continuous TiN layer provides optimal protection, reducing wear by more than one order of magnitude. At the highest power (90%), further hardness increase does not necessarily improve wear resistance, particularly in Grade 4, where signs of brittle damage become evident.

The dominant wear mechanisms evolve with increasing laser power. At low power, adhesive wear combined with abrasive ploughing dominates due to insufficient surface hardening and strong metal-to-metal contact. At intermediate power levels, the presence of a continuous TiN-rich layer promotes a transition toward mild abrasive wear with reduced plastic deformation. At the highest power level, localized brittle fracture and micro-spallation of the compound layer may occur, particularly in Grade 4, indicating that excessive hardness combined with residual stresses can reduce layer integrity under cyclic loading.

These observations demonstrate the existence of an optimal processing window in which compound layer thickness, hardness gradient, and structural integrity are balanced to achieve maximum tribological performance.

4. Conclusions

Surface laser processing of cpTi Grade 2 and cpTi Grade 4 under a high-purity nitrogen jet successfully produced TiN-based compound layers with thicknesses strongly dependent on laser power. A clear transition from a diffusion-dominated regime at 30% power to a melt-dominated reactive regime at ≥50% power was identified for both alloys.

The compound layer thickness increased nonlinearly with laser power, reaching ~45 µm in Grade 2 and ~48 µm in Grade 4 at 90% power. XRD analysis confirmed the formation of TiN as the dominant phase in all treated conditions, with increasing peak intensity corresponding directly to compound layer growth. Minor oxide contributions were detected but did not dominate the phase constitution.

Cross-sectional microhardness profiles revealed significant near-surface strengthening, with maximum hardness values reaching ~1675 HV for Grade 2 and ~1809 HV for Grade 4. While peak hardness tended to plateau at high power, the depth of the hardened region increased substantially with compound layer thickness, demonstrating the importance of subsurface load support.

Wear testing showed a strong correlation between tribological performance and compound layer integrity. Volume loss decreased by up to ~96% in Grade 2 and ~95% in Grade 4 compared to low-power conditions. Optimal wear resistance was achieved at intermediate-to-high laser powers (50-70%), where a thick, continuous TiN-rich layer provided both high surface hardness and sufficient structural integrity. At excessive power (90%), particularly in Grade 4, wear resistance did not improve

proportionally, indicating that residual stress and potential brittleness must be considered in process optimization.

Overall, the results demonstrate that laser processing under nitrogen enables the formation of a functionally graded TiN-based surface layer on commercially pure titanium alloys. The tribological performance is governed primarily by compound layer thickness and hardness gradient continuity rather than peak surface hardness alone. An optimal processing window exists in which surface hardness, layer integrity, and wear resistance are maximized without compromising structural stability.

Acknowledgements

This research was supported by the Bulgarian National Science Fund under the 2024 programme for fundamental scientific research through the project "Laser-induced formation of oxynitride nanostructures on biomedical titanium alloys" (KP-06-PN87/7, BG-175467353-2024-11-0035).

REFERENCES

[1] E. Marin, A. Lanzutti, Biomedical Applications of Titanium Alloys: A Comprehensive Review. Materials (Basel) **17**, (2023). DOI: https://doi.org/10.3390/ma17010114

[2] L. Zhang, L. Chen, A Review on Biomedical Titanium Alloys: Recent Progress and Prospect. Adv. Eng. Mater. **21** (2019). DOI: https://doi.org/10.1002/adem.201801215

[3] B.E. Nagay, J.M. Cordeiro, V.A.R. Barão, Alloy Materials for Biomedical Applications. Alloy Materials and Their Allied Applications, Wiley, 159-189 (2020). DOI: https://doi.org/10.1002/9781119654919.ch9

[4] X. Liu, S. Chen, J.K.H. Tsoi, J.P. Matinlinna, Binary titanium alloys as dental implant materials – a review. Regen. Biomater. **4**, 315-323 (2017). DOI: https://doi.org/10.1093/rb/rbx027

[5] E. Abakay, M. Armağan, Y. Yıldıran Avcu, M. Guney, B.F. Yousif, E. Avcu, Advances in improving tribological performance of titanium alloys and titanium matrix composites for biomedical applications: a critical review. Front. Mater. **11** (2024). DOI: https://doi.org/10.3389/fmats.2024.1452288

[6] S. Kaur, K. Ghadirinejad, R.H. Oskouei, An Overview on the Tribological Performance of Titanium Alloys with Surface Modifications for Biomedical Applications. Lubricants **7**, 65 (2019). DOI: https://doi.org/10.3390/lubricants7080065

[7] N. Xiao, J. Tang, S. Zhou, Y. Shi, F. Qian, S. Qiu, Y. Chen, D. Zhao, K. Yang, Current research on the design, properties and applications of tribological materials: a review. RSC Adv. **15**, 34669-34717 (2025). DOI: https://doi.org/10.1039/d5ra02780b

[8] S. Izman, M. Rafiq, M. Anwar, E.M. Nazim, R. Rosliza, A. Shah, M.A. Hass, Surface Modification Techniques for Biomedical Grade of Titanium Alloys: Oxidation, Carburization and Ion Implantation Processes. Titanium Alloys - Towards Achieving Enhanced Properties for Diversified Applications, InTech (2012). DOI: https://doi.org/10.5772/36318

[9] A. Edrisy, K. Farokhzadeh, Plasma Nitriding of Titanium Alloys. Plasma Science and Technology - Progress in Physical States and Chemical Reactions, InTech (2016). DOI: https://doi.org/10.5772/61937

[10] O.I. Yaskiv, I.M. Pohrelyuk, V.M. Fedirko, D.B. Lee, O.V. Tkachuk, Formation of oxynitrides on titanium alloys by gas diffusion treatment. Thin Solid Films **519**, 6508-6514 (2011). DOI: https://doi.org/10.1016/j.tsf.2011.04.219

[11] T.N. Baker, Laser surface modification of Ti alloys. Woodhead Publishing (2009).

[12] J.C. Colombo-Pulgarín, C.A. Biffi, M. Vedani, D. Celentano, A. Sánchez-Egea, A.D. Boccardo, J.P. Ponthot, Beta Titanium Alloys Processed By Laser Powder Bed Fusion: A Review. J. Mater. Eng. Perform. **30**, 6365-6388 (2021). DOI: https://doi.org/10.1007/s11665-021-05800-6

[13] M.C. Rossi, J.M. Amado, M.J. Tobar, A. Vicente, A. Yañez, V. Amigó, Effect of alloying elements on laser surface modification of powder metallurgy to improve surface mechanical properties of beta titanium alloys for biomedical application. J. Mater. Res. Technol. **14**, 1222-1234 (2021). DOI: https://doi.org/10.1016/j.jmrt.2021.07.037

[14] V. Vallejo-Otero, N. Crespo-Monteiro, E. Gamet, N. Ollier, C. Donnet, A. Valour, Y. Jourlin, Advancements in nitridation of TiO2 layers: Mechanisms, techniques, and applications for TiN thin films. J. Eur. Ceram. Soc. **45**, 117330 (2025). DOI: https://doi.org/10.1016/j.jeurceramsoc.2025.117330

[15] X. Zong, H. Wang, H. Tang, X. Cheng, X. Tian, X. Ran, Microstructure evolution and mass transfer behavior during multi-pass laser surface nitriding process on titanium alloy. Surf. Coat. Technol. **466**, 129565 (2023). DOI: https://doi.org/10.1016/j.surfcoat.2023.129565

[16] C.W. Chan, S. Lee, G.C. Smith, C. Donaghy, Fibre laser nitriding of titanium and its alloy in open atmosphere for orthopaedic implant applications: Investigations on surface quality, microstructure and tribological properties. Surf. Coat. Technol. **309**, 628-640 (2017). DOI: https://doi.org/10.1016/j.surfcoat.2016.12.036